NMR study of the electronic properties and crystal structure of the semiconducting compound Al_2Ru

E. A. Hill
Department of Physics and Astronomy, University of North Carolina, Chapel Hill, North Carolina 27599

P. Volkov and S. J. Poon
Department of Physics, University of Virginia, Charlottesville, Virginia 22901

Y. Wu
Department of Physics and Astronomy, University of North Carolina, Chapel Hill, North Carolina 27599
(Received 3 October 1994)

The nontetrahedral semiconductor Al_2Ru has been studied by ^{27}Al nuclear magnetic resonance from room temperature to 1200 K. An anomalously large ^{27}Al chemical shift of 313 ppm was observed. The ^{27}Al nuclear-spin-lattice relaxation rate is extremely slow at room temperature and significantly increases above 500 K. Analysis of these data is consistent with a very low residual density of states at the Fermi level and a narrow band gap. In addition, high-resolution magic-angle-spinning ^{27}Al spectra show that there are two similar but distinguishable aluminum sites, indicating that the actual crystal structure differs slightly from the one determined by x-ray diffraction.

I. INTRODUCTION

Most well-known semiconductors have covalent bonds with tetrahedrally coordinated local environments such as Si, GaAs, AlP, and CdSe. Nontetrahedral semiconductors also exist. These materials possess a wide variety of compositions, structures, and physical properties, and are of considerable theoretical and technological interest.[1] One such nontetrahedral compound is Al_2Ru, which has been found to exhibit a semiconductinglike gap of 0.17 eV by electrical measurements.[2,3] Al_2Ru, which has the $TiSi_2$ structure, belongs to a class of crystal structures known as Nowotny chimney-ladder structures.[4] The structure of Al_2Ru can be generated by stacking layers of a hexagonal net which is decorated with the Al (ladder) atoms at the vertices and the Ru (chimney) atoms at the centers of the hexagons. The stacking positions and stacking sequence prevent two Ru atoms from ever being nearest neighbors in this structure. The electronic structure of Al_2Ru has been the focus of current theoretical calculations which demonstrate that the formation of a band gap at the Fermi level results from the hybridization between *sp* orbitals of Al atoms and *d* orbitals of Ru atoms.[5] Several issues, however, remain unclear. Electrical and specific-heat measurements fail to yield reliable estimations of the residual electronic density of states (DOS) at the Fermi level because of the presence of impurities and defects. In fact, the apparent DOS at the Fermi level and the carrier density determined from these techniques are quite high.[3] Furthermore, it is difficult to make an accurate theoretical estimation of the very low DOS at the Fermi level because of the approximations employed in theoretical calculations.

Nuclear magnetic resonance (NMR) is a method which probes local properties, and ^{27}Al NMR should be able to provide information about the DOS at the Fermi level through spin-lattice relaxation measurements. The presence of localized defect states such as defects near the grain boundaries and impurity phases will not influence NMR measurements. Here we report the estimation of the DOS at the Fermi level based on ^{27}Al NMR measurements of spin-lattice relaxation time (T_1). It was found that the DOS at the Fermi level in Al_2Ru is about 100 times smaller than the free-electron value. Furthermore, a very large chemical shift of 313 ppm, probably the largest ever reported for ^{27}Al, was observed, indicating the presence of a very narrow band gap. Finally, the magic-angle-spinning (MAS) technique was used to obtain a high-resolution ^{27}Al spectrum. Two well-resolved lines with equal intensity were observed proving the presence of two inequivalent crystallographic Al sites. This is in disagreement with the face-centered orthorhombic D_{2h}^{24} structure which has only one crystallographic Al site as determined by x-ray diffraction.

It should be noted that high-quality icosahedral alloys, such as $Al_{65}Cu_{20}Ru_{15}$, resemble Al_2Ru in many ways including the composition, low electrical conductivity, and low DOS at the Fermi level. The *sp-d* hybridization plays an important role in the formation of both the pseudogap in $Al_{65}Cu_{20}Ru_{15}$ and the band gap in Al_2Ru. The knowledge of NMR properties in Al_2Ru may provide valuable insight into the properties of quasicrystals.

II. EXPERIMENT

The Al_2Ru sample was cut from an ingot made by melting together pure ($>99.95\%$) elements, annealed at 940 °C for 12 h, and quenched in water.[3] Sample phase purity was verified by powder x-ray diffraction.[3] A

home-built high-temperature probe was used to conduct the NMR experiments with a Chemagnetics CMX400 spectrometer at 9.4 T. The ^{27}Al $\frac{1}{2}\leftrightarrow-\frac{1}{2}$ central transition was observed at 104.23 MHz with a Hahn echo pulse sequence (to avoid ringing). Nuclear spin-lattice relaxation rates were obtained with the technique of inversion recovery; selective, uniform irradiation of the central transition was used by employing $\pi/2$ pulses of 6 μs to avoid significant excitation of satellite transitions. Recycle delays of at least 5 times the spin-lattice relaxation time T_1 were used in all of the experiments to insure accurate magnetization measurements. The high-temperature probe uses a noninductively wound resistive heating element with a water-cooled exterior and a molybdenum sample coil fitted for vacuum-sealed quartz sample tubes. The high-resolution MAS experiments were performed with a Chemagnetics 3.2-mm Pencil-2 probe with spinning speeds up to 25 kHz. The MAS spectra were detected by the Hahn-echo technique where the $\pi/2$ and π pulses were synchronized with the rotor of the MAS probe. The ^{27}Al chemical shift of aqueous $Al(NO_3)_3$ was used as a shift reference.

III. RESULTS

Figures 1(a) and 1(b) show the static ^{27}Al spectra of Al_2Ru at room temperature and 973 K, respectively. Both spectra, similar in line shape, clearly exhibit a powder pattern. Contributions to such a line shape may originate from the quadrupolar broadening, the chemical shift anisotropy (CSA), and the anisotropic Knight shift. The latter two broadening mechanisms can be eliminated by the MAS technique, whereas the quadrupolar broadening is reduced but not eliminated by MAS. Figures 2(a), 2(b), and 2(c) show ^{27}Al MAS spectra with spinning rates of 11.2, 15.0, and 24.3 kHz, respectively. The markers (|) in Figs. 2(a), 2(b), and 2(c) indicate true peaks, and the other peaks are spinning sidebands. The doublet in the MAS spectra is due to the presence of two crystallographically inequivalent sites with a ratio 1:1. This doublet is not the MAS powder pattern of the residual second-order quadrupolar broadening. This becomes obvious upon observing that the line shapes of the centerbands and the spinning sidebands vary significantly as a function of the MAS spinning rate. The spinning sidebands associated with the peak at the higher resonance frequency (peak No. 1) are distributed asymmetrically at low spinning rates and have an envelope resembling a CSA powder pattern with an asymmetry parameter $\eta_{CS}=0$.

The upper limit of the magnitude of the quadrupole interaction can be obtained through the MAS residual linewidth, which is 2.2 kHz for each peak. The estimated upper limit of the quadrupole frequency $\upsilon_Q\equiv 3e^2qQ/2I(2I-1)h$ is about 0.75 MHz for both peaks. Thus the quadrupolar broadening (about 10 kHz in static linewidth) alone is too small to account for the very broad static powder pattern shown in Fig. 1(a). As will be discussed below, spin-lattice relaxation measurements indicate that the contribution of the Knight shift to the line shape is also negligible. Consequently, there is

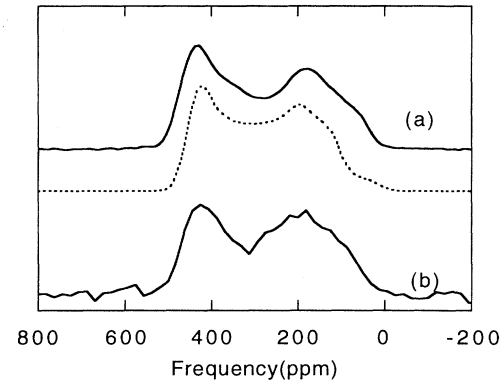

FIG. 1. ^{27}Al spectra of Al_2Ru at (a) room temperature and (b) 973 K. The dashed line is a powder-pattern simulation of the room-temperature spectrum using the parameters given in Table I.

a significant contribution to the powder pattern from the CSA. The contribution of the chemical shift to the powder pattern can be described as

$$\upsilon_{CS}(\text{ppm})=\delta_{CS}^{iso}+\tfrac{1}{2}\delta_{CSA}\eta_{CS}\cos(2\phi)\sin^2\theta\ , \quad (1)$$

where δ_{CS}^{iso} is the isotropic chemical shift, δ_{CSA} is the constant of the CSA, η_{CS} is the asymmetry parameter of the chemical shift tensor, and (θ,ϕ) are the polar angles of the static external magnetic field with respect to the principal axes system (PAS) of the chemical shift tensor. In addition to δ_{CS}^{iso}, quadrupole interactions also contribute to the measured isotropic shift through a second-order effect given by

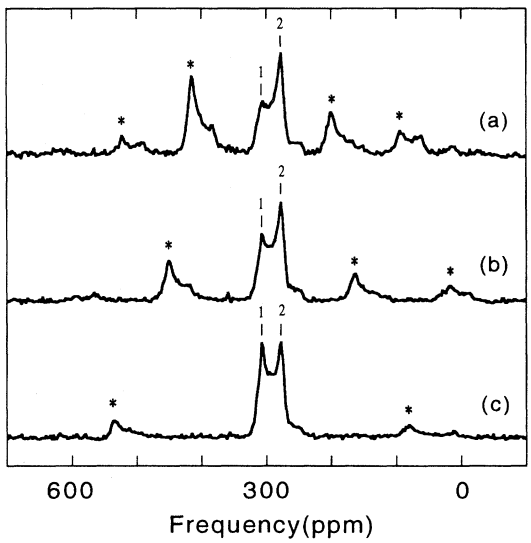

FIG. 2. ^{27}Al magic-angle-spinning spectra of Al_2Ru at spinning rates (a) 11.2, (b) 15.0, and (c) 24.3 kHz. The markers indicate the centerbands of peak Nos. 1 and 2. Unmarked peaks are spinning sidebands; the * symbols indicate spinning sidebands associated with peak No. 1.

$$\delta_{\rm iso}^{(2)} = -\frac{1}{30}\frac{\nu_Q^2}{\nu_L}\left[1+\frac{\eta_Q^2}{3}\right]\left[I(I+1)-\frac{3}{4}\right], \qquad (2)$$

where ν_L is the Larmor frequency and η_Q is the asymmetry parameter of the electrical-field-gradient (EFG) tensor. Given the chemical shift tensor, the EFG tensor, and the Euler angles (α,β,γ) which transform the PAS of the EFG tensor into the PAS of the chemical shift tensor, the static line shape can be simulated. The dashed line in Fig. 1 shows a powder-pattern simulation of the room-temperature static spectrum. Parameters used for the simulation are listed in Table I. Despite the large number of parameters involved in this simulation, several aspects of the simulation are unambiguous because of the constraints provided by the MAS spectra. It is clear that the two peaks have equal intensity. Both peaks have very large chemical shifts, and the $\eta_{\rm CS}$ value for peak No. 1 is close to zero. The isotropic chemical shift of peak No. 1 is 313 ppm and, to our knowledge, is the largest chemical shift ever reported for ^{27}Al.

There are other intriguing NMR properties of Al_2Ru such as spin-spin interactions and spin-lattice relaxations. Since anisotropic broadenings dominate the linewidth as discussed above, spin-spin interactions can only be measured through the decay of the Hahn echo as a function of the time spacing $\tau_{\rm echo}$ between the $\pi/2$ and π pulses. Figure 3 is a plot of the normalized magnetization $M_{\rm echo}$ versus the total dephasing time $2\tau_{\rm echo}$. The decay follows an exponential function over several orders of magnitude. The solid line is a single exponential fit with a time constant T_2 of 385 μs. The spin-spin relaxation keeps this exponential form up to a temperature $T=1073$ K, and the time constant of the exponential function gradually decreases by about 30% over this temperature range, as seen in Fig. 4. Atomic diffusion can reduce T_2 by changing the local environments over the time scale of $\tau_{\rm echo}$. However, the observed decrease of T_2 at high temperature is very gradual and small; this indicates that significant atomic diffusion does not occur at the observed temperatures.

Figure 5 shows the room temperature (296 K) inversion-recovery data for the ^{27}Al magnetization in Al_2Ru. The data are plotted as M^* versus the recovery time τ, where M^* is defined by $M^* \equiv [M_\infty - M(\tau)]/(M_\infty - M_0)$. M_∞ is the equilibrium magnetization, M_0 is the magnetization immediately after the magnetization inversion (more than 90% inversion), and $M(\tau)$ is the magnetization at the recovery time τ. The recovery of the magnetization for the central transition of half-integer quadrupolar nuclei follows a multiple-exponential function. In the case of dipolar relaxation

TABLE I. Room-temperature static line-shape simulation parameters.

Peak	$\delta_{\rm CS}^{\rm iso}+K^0$ (ppm)	$\delta_{\rm CSA}$ (ppm)	$\eta_{\rm CS}$	ν_Q (MHz)	η_Q	α	β	γ
No. 1	323	250	0.2	0.75	1.0	0°	15°	0°
No. 2	292	230	1.0	0.75	1.0	45°	90°	90°

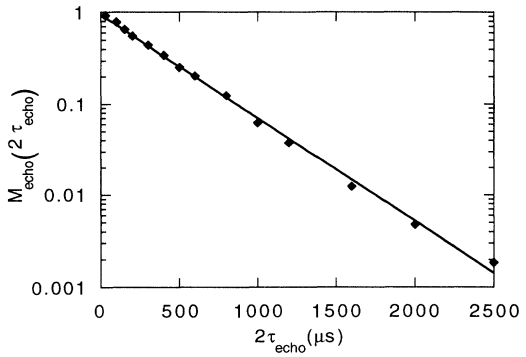

FIG. 3. ^{27}Al spin-echo height $M_{\rm echo}$ vs echo dephasing time $2\tau_{\rm echo}$ at room temperature. The solid line is a fit corresponding to a single exponential with a time constant of 385 μs.

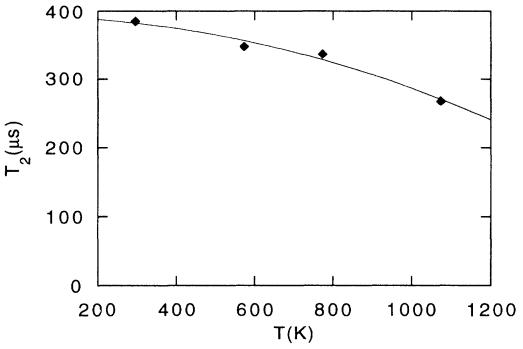

FIG. 4. The spin-spin relaxation time T_2 vs temperature. T_2 was determined by an exponential fit to the spin-echo data at each temperature. The solid line is only a guide for the eye.

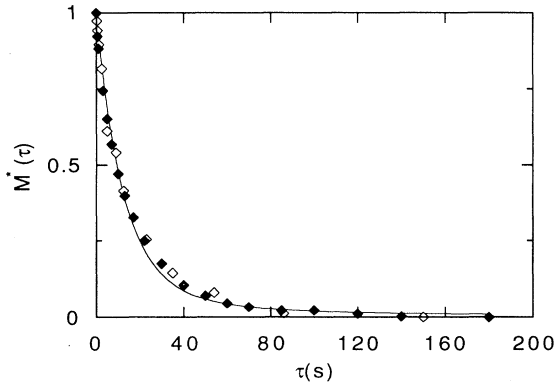

FIG. 5. Function M^* (see text) vs the magnetization recovery time τ. The solid symbols are the actual room-temperature data; the open symbols correspond to the data at 1073 K where the τ axis has been scaled by a factor of 100. The solid line is a fit based on Eq. (3) of the text.

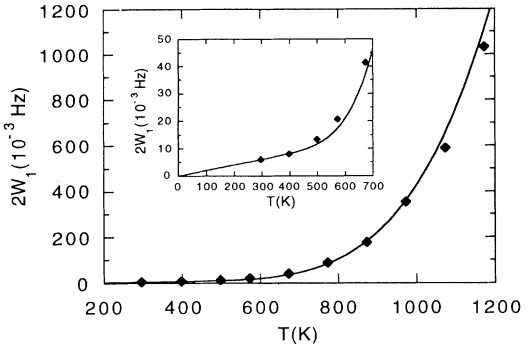

FIG. 6. The spin-lattice relaxation rate $2W_1$ vs temperature. The inset shows the region below 700 K. The solid line is the fit based on Eq. (10), which is described in the text.

mechanisms, such as Korringa relaxation, the inversion recovery of the central transition for spin-$\frac{5}{2}$ nuclei is described by,[6]

$$M(\tau)=M_\infty[1-0.057\exp(-2W_1\tau) -0.356\exp(-12W_1\tau) -1.587\exp(-30W_1\tau)] . \quad (3)$$

The spin-lattice relaxation time T_1 is defined as $T_1\equiv 1/(2W_1)$. The solid line in Fig. 5 is a fit using Eq. (3) with $T_1=169$ s. The temperature dependence of the relaxation rate $2W_1$ is displayed in Fig. 6. The functional form of the M^* versus τ curve remains identical over the whole temperature range of our measurements. The M^* versus τ plots from all temperatures overlap with each other after the scaling of the τ axis with a corresponding scaling factor. An example is given in Fig. 5, where the recovery curve of M^* at 1073 K is shown after the τ axis is scaled by a factor of 100. Notice the extremely long ^{27}Al spin-lattice relaxation time T_1 in Al_2Ru. For comparison, T_1 at room temperature in pure aluminum metal is 6.3 ms.

IV. DISCUSSION

A. The density of states

There are various mechanisms of spin-lattice relaxation in metals and alloys. The most common one is the Korringa relaxation mechanism which originates from the contact term of the hyperfine coupling between the nuclear spins and unpaired electron spins. This mechanism is characterized by a linear temperature dependence of the relaxation rate given by

$$\frac{1}{T_1}=\tfrac{64}{9}\pi^3\hbar^3k_B\gamma_e^2\gamma_n^2\langle|u_k^2(0)|\rangle_{E_F}^2 g(E_F)^2T , \quad (4)$$

where $\langle|u_k^2(0)|\rangle_{E_F}$ is the density of the wave function at the nucleus averaged over the Fermi surface, $g(E_F)$ is the DOS for a single-spin orientation at the Fermi level E_F, γ_e and γ_n are the gyromagnetic ratio of the electron and the observed nucleus, respectively, and k_B is the Boltzmann constant. As expected, a nearly free-electron metal with a relatively large $g(E_F)$ value, such as pure aluminum, has an extremely short T_1 at room temperature ($T_1^{Al}=6.2$ ms). Al-TM (transition metal) alloys which have a more complex DOS, such as trigonal Al_7Cu_2Fe, have a longer room-temperature T_1 value ($\sim$95 ms) due to a reduced $g(E_F)$ value.[7] In the present case, Al_2Ru has a room-temperature T_1 value of $T_1^{Al_2Ru}=169$ s, and the spin-lattice relaxation rate below 400 K can be characterized by a function linear in T corresponding to a value of $T_1^{Al_2Ru}T=5\times10^4$ s K (whereas $T_1^{Al}T=1.85$ s K). Equation (4) can be used to evaluate the value of the DOS at the Fermi level by writing

$$g^{Al_2Ru}(E_F)=\frac{g^{Al}(E_F)\sqrt{T_1^{Al}T}}{\xi^{Al_2Ru}\sqrt{T_1^{Al_2Ru}T}} . \quad (5)$$

Here $\xi^{Al_2Ru}=\langle|u_k^2(0)|_{Al_2Ru}\rangle_{E_F}\langle|u_k^2(0)|_{Al}\rangle_{E_F}^{-1}$ is a parameter which describes the character of the wave function at the aluminum sites in Al_2Ru. Values of $\xi^{Al_2Ru}<1$ indicate diminished s character relative to pure aluminum. The value $g^{Al}(E_F)=3.2\times10^{22}$ cm^{-3}eV^{-1} gives an estimate of $g^{Al_2Ru}(E_F)=2\times10^{20}$ cm^{-3}eV^{-1}, assuming $\xi^{Al_2Ru}=1$. The DOS at the Fermi level could be higher if the wave functions at the Fermi level in Al_2Ru contain less s character than the corresponding wave functions in aluminum metal. The stated DOS value, therefore, should be taken as an order-of-magnitude estimate rather than an exact value. It should also be mentioned that two other parts of the hyperfine coupling which can contribute to the spin-lattice relaxation, the orbital relaxation and dipolar relaxation, have been neglected in the above calculation. Both of these mechanisms depend on the square of $g(E_F)$ like the Korringa mechanism, yet an additional dependence on the inverse-sixth power of the electron-nucleus distance makes their contribution to the total relaxation relatively small in lighter elements such as aluminum.[8] Furthermore, quadrupolar relaxation mechanisms (due to EFG fluctuations caused by phonons and atomic diffusion) have been neglected in this temperature regime upon consideration of the observed linear temperature dependence which is a signature of the Korringa mechanism. Contributions to the spin-lattice relaxation by any mechanisms other than the Korringa mechanism would make the above $g^{Al_2Ru}(E_F)$ value an overestimate because the rates are additive.

B. The Knight shift and the chemical shift

The relaxation data also allow an estimation of the contribution of the contact term to the resonance shift, known as the isotropic Knight shift, given by

$$K^0=\tfrac{4}{3}\pi\hbar^2\gamma_e^2\langle|u_k^2(0)|\rangle_{E_F}g(E_F) . \quad (6)$$

$K^0_{Al_2Ru}$ can be determined to be about 10 ppm from $T_1^{Al_2Ru}T(K^0_{Al_2Ru})^2=T_1^{Al}T(K^0_{Al})^2$ and $K^0_{Al}=1600$ ppm. This is an extremely small Knight shift for ^{27}Al in a

metal-based compound. A second-order isotropic quadrupolar shift of $\delta_{iso}^{(2)}=-15$ ppm has been determined from Eq. (2) by using the quadrupolar frequency found for both sites in the powder-pattern simulation of the line shape. The remaining contributions of +313 and +282 ppm to the total shift values of the two peaks observed under MAS must be accounted for by the orbital term of the hyperfine interaction, which can give rise to paramagnetic (as well as diamagnetic) shifts. The orbital hyperfine shift, known as the chemical shift, has been found to take on values in the relatively limited range of −225 to +221 ppm for ^{27}Al in aluminum compounds;[9] as mentioned above, orbital effects are somewhat diminished for a lighter element because of their dependence on the average electron-nucleus distance.[10] Exceptions, however, are expected in a narrow-gap semiconductor. The equation for the paramagnetic orbital shift can be calculated from second-order perturbation theory as[11]

$$\sigma_p=\frac{2\mu_B^2}{3}\sum_{k=1}^{N}\langle 0|(\mathbf{L}\cdot C\boldsymbol{l}_k+\boldsymbol{l}_k\cdot C\mathbf{L})r_k^{-3}|0\rangle\ , \tag{7}$$

where μ_B is the Bohr magneton, the sum is over N electrons, $\langle 0|$ is the electronic ground state, $\mathbf{L}$ is the total orbital angular momentum, $\boldsymbol{l}_k$ is the orbital angular momentum of the kth electron, r_k is the distance from the nucleus to the kth electron, and the operator C is defined as $C=\sum_n'|n\rangle\langle n|(E_0-E_n)^{-1}$, where the $\langle n|$'s are the electronic excited states, E_0 is the ground-state energy, and E_n's are the energies of excited states. It is worthwhile to note that the orbital shift is influenced by all states and there is no factor of $g(E_F)$ in Eq. (7), unlike the orbital relaxation mechanism which depends on the existence of unpaired electron spins near the Fermi level. An actual determination of σ_p in materials with a complex band structure such as Al_2Ru is formidable at best, yet Eq. (7) provides a qualitative explanation of the large paramagnetic shifts which have been observed here. If the major contribution to σ_p results from excited states confined in a narrow energy range in the DOS, a narrow band gap often implies a small energy splitting between the ground state and these excited states. This makes the factors $(E_0-E_n)^{-1}$, thus also σ_p, large. Therefore, the observed large chemical shifts are consistent with the existence of a narrow energy gap in Al_2Ru.

The existence of two resonance lines is not consistent with the structures determined by x-ray diffraction. An ideal $TiSi_2$ structure must have an orthorhombic unit cell with a b/a ratio of 0.577, where a and b are unit-cell dimensions, in order for the lattice layers to contain perfect hexagons.[4] A different value of the b/a ratio, 0.588 for Al_2Ru, indicates an elongation of the hexagons. However, this still does not explain why there are two equally abundant crystallographically inequivalent sites as observed by MAS NMR. The shift difference indicates a slight difference of electronic structure between the two sites due to a deviation from the proposed structure. The mechanism and degree of this distortion is an open question.

C. The spin-spin relaxation

As mentioned above, the behavior of spin-spin relaxations in Al_2Ru is unusual. In general, Van Vleck's moment analysis is very useful for analyzing the line shape and spin-spin-relaxation time. For instance, the ^{27}Al linewidth in pure aluminum can be explained by nuclear dipolar interactions through the calculation of the second moment given by

$$M_2=\tfrac{3}{5}\gamma^4\hbar^2I(I+1)\sum_k\frac{1}{r_{jk}^6}\ , \tag{8}$$

where the sum is over the lattice positions of like nuclei (k) separated by r_{jk} from a chosen nucleus (j).[12] Calculations yield a value of $M_2^{Al}=9.1\times10^6$ Hz^2 for pure aluminum and a value of $M_2^{Al_2Ru}=7.6\times10^6$ Hz^2 for the Al_2Ru structure assuming, erroneously, that all of the Al lattice sites in Al_2Ru are equivalent and that the magnetic Zeeman sublevels are not split by the first-order quadrupolar interaction. Since the line shape of the ^{27}Al resonance in pure aluminum is nearly Gaussian, the second moment can be directly linked to the observed linewidth at half maximum $\Delta\nu_{1/2}$.[13] The observed linewidth value for pure aluminum is 9.5 kHz, and the calculated value is 7.1 kHz. In the present experiment, the spin-spin interaction is determined through the Hahn-echo decay, and the Zeeman sublevels are split by the first-order quadrupolar interaction. As a result, the value of the second moment should be reduced by a factor of $\frac{41}{107}$ for spin-$\frac{5}{2}$ nuclei.[14] As mentioned above, Fig. 3 shows that the nuclear-spin-spin-relaxation process for ^{27}Al in Al_2Ru is well described by an exponential function with a time constant of 385 μs; this data cannot be directly linked to the calculated second moment because of the divergence of the second moment associated with a Lorentzian line shape. Considering the very similar second moments calculated for pure aluminum and Al_2Ru, the marked difference in the rate and functional form of their spin-spin relaxation is a surprising result. The presence of two well-resolved lines in Al_2Ru can be partially responsible for this observation. The differences both in chemical shift as well as quadrupole interactions serve to suppress the spin-flip-flop interactions between spins at the two different local environments (crystallographically inequivalent sites associated with peak Nos. 1 and 2). It is clear that significant suppression of flip-flop interactions is expected if each aluminum site (e.g., corresponding to peak No. 1) is different from its nearest neighbors (e.g., corresponding to peak No. 2). This situation is essentially the same as spin-spin interactions between heteronuclear spins where flip-flop interactions are suppressed. Heteronuclear spin-spin interactions cause a decrease of the ratio $\sqrt{M_2^2/M_4}$, where M_4 is the fourth moment.[15] This effect, which makes the line shape more Lorentzian, is large if the off-resonant nuclei have a much larger gyromagnetic ratio than the resonant nuclei.[11] Obviously, this is not the case here because both types of nuclei involved are ^{27}Al nuclei. Thus it would be surprising if the suppression of flip-flop interactions in Al_2Ru is sufficient to make the echo-height decay perfectly ex-

ponential. Isotropic indirect couplings much larger than dipolar interactions can also make T_2 longer and decay of the echo height more exponential.[11] Isotropic indirect couplings between spins at different local environments contribute to the MAS linewidths, which are quite narrow for peak Nos. 1 and 2 (about 2.2 kHz); thus isotropic indirect couplings in Al_2Ru are smaller than dipolar interactions and cannot be responsible for the exponential decay. A more satisfactory explanation is needed for the observed perfect exponential decay.

A study of the temperature dependence of the nuclear-spin-spin relaxation can provide information about the time scale of diffusive atomic motion in the lattice. Figure 4 shows that there is a relatively small decrease in T_2 for Al_2Ru across the measured temperature range. Motion characterized by a correlation time τ_c on the order of the echo delay τ_{echo} (about 1 ms) can cause changes in the local fields before and after the π refocusing pulse; the refocusing is less effective causing a decrease in T_2. Very fast motions on the time scale of the Larmor frequency (about 10 ns) can also contribute to T_2 through the changes of T_1. Since $1/T_1$ is much smaller than $1/T_2$ even at the highest temperature measured, the contribution of spin-lattice relaxation to the spin-spin relaxation can be neglected. Changes of local environments on the time scale of the inverse of the linewidth (about 20 μs) or faster can cause significant changes of the line shape. The line shape remains essentially identical up to 973 K, and such fast motions seem to be nonexistent. This result is not surprising, as the melting point for Al_2Ru is over 2000 K.[2]

D. The spin-lattice relaxation at high temperature

Motion-induced EFG fluctuations cause spin-lattice relaxation for quadrupolar nuclei, yet it is not quite clear, for the moment, what effect the motions detected by the spin-spin relaxation have on the spin-lattice relaxation in Al_2Ru, in particular at high temperatures where $1/T_1$ increases sharply (Fig. 6). Although evidence shows that fast motions on the time scale of the Larmor frequency are insignificant here, a model of the diffusion processes in Al_2Ru and the influences on the EFG fluctuations are needed for any definitive answer. So far, the possibility of motion-induced spin-lattice relaxation in the high-temperature range of our experiments cannot be excluded.

Another possible explanation attributes the sharp increase of $1/T_1$ to thermally excited electrons from the valence band to the conduction band at high temperatures. Based on the theoretical calculations mentioned earlier,[5] the conduction-band DOS near the bottom of the conduction band E_c can be roughly approximated by $g(E)=G(E-E_c)$, with $G=1\times10^{22}$ cm^{-3} eV^{-2}, when $E>E_c$ and $g(E)=0$ when $E<E_c$. In this case, the contact term of the hyperfine coupling between the nuclear spins and the excited unpaired electron spins in the conduction band leads to spin-lattice relaxations given by[16]

$$\frac{1}{T_1}=\frac{64}{9}\pi^3\hbar^3 k_B\gamma_e^2\gamma_n^2\langle|u_k^2(0)|\rangle_c^2 GNT\ , \tag{9}$$

where N is the number of excited electrons in the conduction band and $\langle|u_k^2(0)|\rangle_c$ is an average of the density of the wave function at the nucleus near the bottom of the conduction band. Comparing with Eq. (4) it can be seen that thermally excited electrons should have a noticeable effect if GN is comparable to $[\langle u_k^2(0)|\rangle_{E_F}^2 g(E_F)^2][\langle|u_k^2(0)|\rangle_c^2]^{-1}$. An estimate of $g^{Al_2Ru}(E_F)=2\times10^{20}$ cm^{-3} eV^{-1} can be taken from the previous discussion. Given the approximate nature of this calculation we assume a value of $\langle|u_k^2(0)|\rangle_{E_F}^2/\langle|u_k^2(0)|\rangle_c^2=10$ because of the significant d-orbital character near the bottom of the conduction band. The result implies that a value of N on the order of 10^{19} cm^{-3} could have a measurable effect on the spin-lattice relaxation. This number of excited electrons is not unusual at high temperatures, particularly considering the sharp increase of the conductivity above 500 K.[3] It follows that N is proportional to $T^2\exp(-E_a/k_BT)$, based on the form of $g(E)=G(E-E_c)$, and curve of $1/T_1$ versus T can be fit with the function

$$\frac{1}{T_1}=AT+BT^3\exp\left[-\frac{E_a}{k_BT}\right]. \tag{10}$$

The first term, which dominates the low-temperature behavior, describes the Korringa relaxation with a constant A. The second term, proportional to a constant B, describes the thermal excitation process of the electrons at higher temperatures; given that the Fermi level is predicted to be at the top of the valence band, E_a is a measure of the band gap. The best fit is shown in Fig. 6 with $E_a=0.3$ eV. It should be noted that gap energies of 0.2 and 0.14 eV have been determined for Al_2Ru by conductivity measurements and theoretical calculations, respectively.[17,5] The value of 0.3 eV determined by Eq. (10) is sensitive to the function chosen to model the DOS near the bottom of the conduction band. For example, replacing T^3 with T^4 in Eq. (10), which corresponds to a parabolic shape for the DOS, would yield a gap value of about 0.2 eV. Furthermore, consequences of the crystallographic modification discussed earlier were not considered in previous theoretical calculations; this introduces another source of uncertainty when comparing experimentally measured gap values with the theoretical gap value cited above. Given the crude nature of the above estimation and the unknown contribution of motion-induced relaxation, further investigations are needed to unambiguously determine the mechanism that causes the sharp increase of $1/T_1$ above 500 K.

V. CONCLUSION

In summary, ^{27}Al NMR has been used to examine the unique electronic properties of the semiconducting crystal Al_2Ru. The extremely long nuclear-spin-lattice relaxation times imply a very low DOS; assuming the percentage of the s-wave character at the Fermi level is comparable to that of pure aluminum, a Fermi-level DOS of 2×10^{20} cm^{-3} eV^{-1} is determined for Al_2Ru. In addition, anomalously large ^{27}Al chemical shifts of 313 and 282

ppm have been measured and are qualitatively consistent with the presence of a narrow band gap. The temperature dependence of the nuclear-spin-spin relaxation time indicates that there is little diffusion up to 800 K. With this in mind, an explanation for the strong increase of the nuclear-spin-lattice relaxation rate above 500 K is given as an alternative to quadrupolar relaxation mechanisms. It was shown that a spin-lattice relaxation process mediated by thermally excited electrons provides a consistent explanation for the high-temperature relaxation data; an activation energy of 0.2–0.3 eV was determined. Finally, high-speed magic-angle-spinning spectra show that there are two similar but distinct aluminum sites. This implies a small deviation of lattice structure from the structure previously determined by x-ray diffraction.

ACKNOWLEDGMENT

This work was supported by the National Science Foundation under Contract Nos. DMR-9122992 and DMR-9319084.

[1]C. H. L. Goodman, Mater. Res. Bull. **20**, 237 (1985).

[2]Semiconducting behavior in Al_2Ru was shown qualitatively by J. Evers, G. Oehlinger, and H. Meyer, Mater. Res. Bull. **19**, 1177 (1984).

[3]F. S. Pierce, S. J. Poon, and B. D. Biggs, Phys. Rev. Lett. **70**, 3919 (1993).

[4]See, for example, W. B. Pearson, *The Crystal Chemistry and Physics of Metals and Alloys* (Wiley, New York, 1972), p. 594.

[5]D. Nguyen Manh, G. Trambly de Laissardiere, J. P. Julien, D. Mayou, and F. Cyrot-Lackmann, Solid State Commun. **82**, 329 (1992).

[6]A. Narath, Phys. Rev. **162**, 320 (1967).

[7]E. A. Hill, T. C. Chang, Y. Wu, S. J. Poon, F. S. Pierce, and Z. M. Stadnik, Phys. Rev. B **49**, 8615 (1994).

[8]J. Winter, *Magnetic Resonance in Metals* (Clarendon, Oxford, 1971), p. 43.

[9]J. W. Akitt, in *Annual Reports on NMR Spectroscopy,* edited by E. F. Mooney (Academic, London, 1972), Vol. 5A, p. 465.

[10]J. J. Spokas, C. H. Sowers, and D. O. Van Ostenburg, Phys. Rev. B **1**, 2523 (1970).

[11]A. Abragam, *The Principles of Nuclear Magnetism* (Clarendon, Oxford, 1961), p. 175.

[12]A. Abragam, *The Principles of Nuclear Magnetism* (Ref. 11), p. 112.

[13]A. Abragam, *The Principles of Nuclear Magnetism* (Ref. 11), p. 107.

[14]J. Haase and E. Oldfield, J. Magn. Res. A **101**, 30 (1993).

[15]J. H. Van Vleck, Phys. Rev. **74**, 1168 (1948).

[16]A. Abragam, *The Principles of Nuclear Magnetism* (Ref. 11), p. 389.

[17]P. Volkov and S. J. Poon, Europhys. Lett. **28**, 271 (1994).